

Article

Synthesis of Nano-Structured Conjugated Polymers with Multiple Micro-/Meso-Pores by the Post-Crosslinking of End-Functionalized Hyperbranched Conjugated Polymers

Zhenfeng Liang and Hui Liang *

Key Laboratory of Designed Synthesis and Application of Polymer Materials (DSAPM Lab), Key Laboratory for Polymer Composite and Functional Materials of Ministry of Education (PCFM Lab), School of Chemistry, Sun Yat-sen University, Guangzhou 510006, China; liangzhf@mail2.sysu.edu.cn

* Correspondence: ceshui@mail.sysu.edu.cn

Abstract: A nano-structured conjugated polymer with multiple micro-/meso-pores was synthesized by post-crosslinking of an end-functionalized hyperbranched conjugated prepolymer. Firstly, an AB₂ monomer 3-((3,5-dibromo-4-(octyloxy)phenyl)ethynyl)-6-ethynyl-9-octyl-9H-carbazole (PPECz) was synthesized and polymerized by Sonogashira reaction to give the -Br end-functionalized hyperbranched conjugated prepolymer *hb*-PPECz. The photophysical and electrochemical properties of *hb*-PPECz were investigated. The λ_{max} of absorption and emission of *hb*-PPECz in tetrahydrofuran (THF) solution was 313 and 483 nm, respectively. The optical energy bandgap, highest occupied molecular orbital (HOMO), and lowest unoccupied molecular orbital (LUMO) energy levels of *hb*-PPECz were 2.98, -5.81, and -2.83 eV, respectively. Then, the prepolymer *hb*-PPECz was post-crosslinked by Heck reaction with divinylbenzene to give the porous conjugated polymer *c*-PPECz. The effects of *hb*-PPECz concentration and added dispersant polyvinylpyrrolidone (PVP K-30) on the morphology and porosity of *c*-PPECz were investigated. The resulting *c*-PPECzs showed multiple porous structures mainly constructed by micropores and mesopores. Under a higher *hb*-PPECz concentration (4 wt/v%), a bulky gel product was obtained. Under lower *hb*-PPECz concentrations (0.6 wt/v%~2 wt/v%), the resulting *c*-PPECzs were mainly composed of nano-sized particles. Nearly spheric nanoparticles (200~300 nm) (*c*-PPECz-5) were obtained under the concentration of 1 wt/v% in the presence of PVP (10 wt% of *hb*-PPECz). The Brunauer–Emmett–Teller (BET) surface area, pore volume, average pore size, and percentage of pore size below 10 nm of *c*-PPECz-5 were $10.7781 \text{ m}^2 \cdot \text{g}^{-1}$, $0.0108 \text{ cm}^3 \cdot \text{g}^{-1}$, 4.0081 nm, and 94.47%, respectively.

Keywords: microporous conjugated polymer; hyperbranched conjugated polymer; post-crosslinking; Sonogashira coupling reaction; Heck reaction



Citation: Liang, Z.; Liang, H. Synthesis of Nano-Structured Conjugated Polymers with Multiple Micro-/Meso-Pores by the Post-Crosslinking of End-Functionalized Hyperbranched Conjugated Polymers. *Polymers* **2024**, *16*, 1192. <https://doi.org/10.3390/polym16091192>

Academic Editor: Ioan Botiz

Received: 3 April 2024

Revised: 19 April 2024

Accepted: 22 April 2024

Published: 24 April 2024



Copyright: © 2024 by the authors. Licensee MDPI, Basel, Switzerland. This article is an open access article distributed under the terms and conditions of the Creative Commons Attribution (CC BY) license (<https://creativecommons.org/licenses/by/4.0/>).

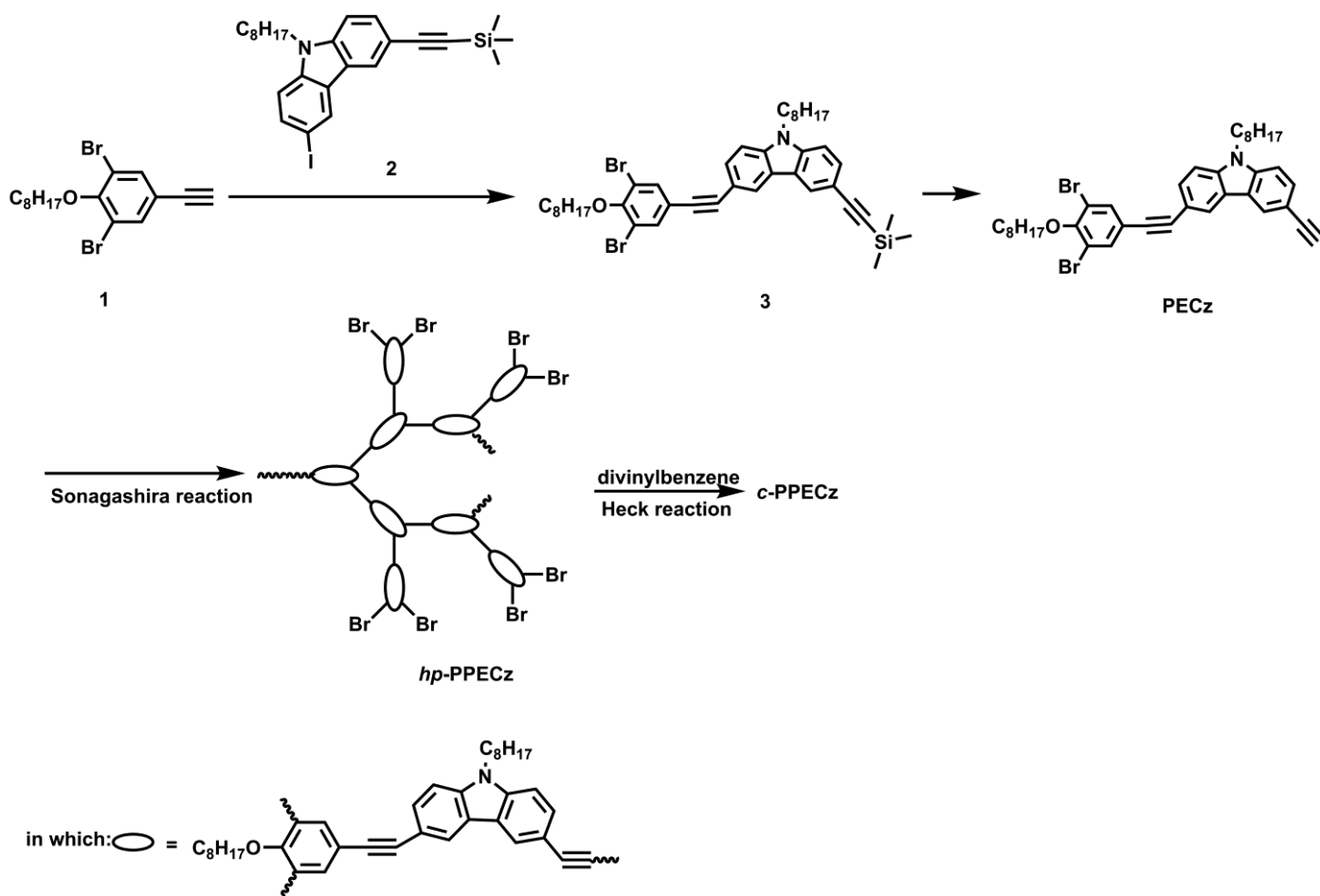
1. Introduction

Conjugated microporous polymers (CMPs) are a class of amorphous materials containing crosslinked conjugated backbones and a great amount of micropores. The combination of conjugated backbones and microporous structures provides not only excellent physicochemical properties but also great pore space to accommodate carriers. Moreover, the crosslinked structure can inhibit the dissolution of the materials. Therefore, CMPs exhibit many advantages over other organic microporous materials and have received increasing attention in the fields of clean energy [1–3], such as hydrogen storage materials [4–6], carbon dioxide capture and conversion [7–10], metal-ion rechargeable batteries [11,12], supercapacitors [13,14], heterogeneous catalysts [15,16], light-harvesting materials [17,18], luminescent materials [19,20], and photovoltaic materials [21,22].

Almost all the reported CMPs were synthesized by A_m + B_n small-molecule monomer systems. The structure and functionality of A_m and B_n were designed to control the structure and photoelectric properties of CMPs, including the morphology, construction of

a porous structure, porosity, and energy gap [2]. CMPs synthesized by $A_m + B_n$ small-molecule monomer systems are typically irregular powder materials and restrict further applications. Other forms of CMPs with nanospherical, nanotubular, thin-film structures were reported to be used in high-performance energy-related applications [2]. Nanospherical CMPs have promising applications in gas storage separation, energy storage, and solar energy conversion. However, the synthesis of nanospherical CMPs is still a great challenge owing to the poor dispersibility and solution processing of CMPs.

Herein, we reported the synthesis of a nano-structured micro-/meso-porous crosslinked conjugated polymer by the post-crosslinking of a -Br end-functionalized hyperbranched conjugated prepolymer via Heck reaction with divinylbenzene. The structures and synthetic route of hyperbranched prepolymer and porous crosslinked conjugated polymer are shown in Scheme 1.



Scheme 1. Structure and synthetic route of hyperbranched prepolymer (*hb*-PPECz) and porous crosslinked conjugated polymer (*c*-PPECz).

Firstly, an AB₂-type monomer (3-((3,5-dibromo-4-(octyloxy)phenyl)ethynyl)-6-ethynyl-9-octyl-9H-carbazole, PECz) constructed by phenyl-, ethynyl-, and carbazole-blocks was synthesized and polymerized to give the hyperbranched conjugated prepolymer *hb*-PPECz. *hb*-PPECz carries -Br group in each branch end. Post-crosslinking of *hb*-PPECz by Heck reaction with divinylbenzene gave crosslinked conjugated polymer *c*-PPECz. It can be expected that porous structures resulting from the free volume between the conjugated branches and crosslinked conjugated skeleton will form in *c*-PPECz. Moreover, using a hyperbranched prepolymer instead of the small molecule as the crosslinking block will result in better solubility of the former, which will generate a swellable gel layer on the surface of the precipitated product. This surface gel layer can act as a volume-

repulsion stabilizer to prevent the agglomeration of gel particles and make it possible to obtain better dispersibility of the resulting *c*-PPECz, resulting in spherical products like in the case of radical precipitation/dispersion polymerization [23,24]. In radical dispersion polymerization, the addition of a dispersant can inhibit agglomeration between the particles better than in radical precipitation polymerization without a dispersant. Therefore, the effect of the added dispersant of PVP K-30 on the morphology and pore structure of the post-crosslinking particles was investigated. By varying the conditions of the post-crosslinking reaction, nano-structured nearly spherical multiple micro-/meso-porous *c*-PPECz with a moderate surface area were obtained. On the other hand, the abundant coordination sites (including C≡C bonds and O, N heteroatoms) provide *c*-PPECz with the ability to complex with metal ions to increase the conductivity and content of active metal species, which can improve the performance of CMPs as electrode materials and electrocatalysts. Therefore, the loading of metal ions into *c*-PPECz was investigated.

2. Experimental Section

2.1. Materials and Instruments

N-iodosuccinimide (98%), 1-bromoocetane (98%), 1,4-diiodobenzene (98%), trimethylsilylacetylene (98%), 2,6-dibromophenol (98%), copper(I) iodide (98%), and bis(triphenylphosphine) palladium chloride (98%) were purchased from Acros Organics. Sodium sulfate anhydrous (99%), sodium chloride (99.5%), potassium hydroxide (95%), 3,6-diiodocarbazole (98%), 2,7-diiodofluorene, palladium acetate (99%), $(O\text{-tolyl})_3\text{P}$ (97%), and diethylbenzene (80% with stabilizer) were purchased from Shanghai Macklin Biochemical (Shanghai, China); dimethyl sulfoxide (99%), ethyl acetate (99%), tetrahydrofuran (99%), methanol (99%), triethylamine (99%), and petroleum ether (99%) were purchased from Shanghai Aladdin Biochemical Technology Co., Ltd. (Shanghai, China) PVP K-30 was purchased from Guangdong Zhuguang New Energy Technology Co., Ltd. (Guangzhou, China) Other reagents were all reagent-grade materials and purified by standard methods if needed.

The scanning electron microscope (SEM) used is the Hitachi High-Technologies S-4800 model (Tokyo, Japan), with an acceleration voltage of 5 kV. The average molecular weight (M_n) and molecular weight distribution (M_w/M_n) of the polymer were determined using an Agilent Technologies PL-GPC 50 gel permeation chromatography system (Bournemouth, UK). The GPC column configuration consisted of an Agilent PL 10 μM MIXED-B gel column followed by two Agilent PL 5 μM MMIXED-D gel columns in series. Polystyrene (PS) was used as a standard sample, and detection was performed with a refractive index detector. The test temperature was maintained at 40 °C, tetrahydrofuran (THF) was used as the mobile phase, and the flow rate was set at 1.0 mL/min.

^1H NMR spectra were recorded on an Avance III 400 MHz NMR spectrometer (Bruker, Fällanden, Switzerland) in CDCl_3 with tetramethylsilane as an internal standard. Chemical shifts were reported in ppm relative to the internal standard. The cyclic voltammograms were recorded on an IM6e electrochemical workstation (German ZAHNER Co., Ltd., Kronach, Germany). The three-electrode system used involved a glassy carbon electrode as the working electrode, calomel electrode as the reference electrode (RE), platinum electrode as the auxiliary electrode (AE), scanning speed of 20 mv/s, polymer sample concentration of 10^{-4} mol/L, using dichloromethane as the solvent, and adding tetrabutylhexafluorophosphate ammonium (0.1 M dichloromethane solution) as the supporting electrolyte.

The instrument used for adsorption–desorption analysis is the Belsorp instrument model BSD-660M A6B3M (Belsorp Instrument Technology Co., Ltd, Beijing, China) series fully automatic surface area and pore size analyzer. The instrument is capable of measuring pore sizes ranging from 3.5 to 5000 angstroms. UV-vis absorption spectra were recorded on a CARY5000 spectrophotometer. Fluorescence spectra were recorded on a Steady State and Transient Fluorescence Spectrometer-1000 (Edinburgh Company, Edinburgh, UK) at an excitation wavelength of 313 nm.

2.2. General Procedures of Syntheses

Compound **1** [25] and Compound **2** [26] were synthesized by the procedures in the literature, respectively.

Synthesis of Compound **3**: 2 g (5.16 mmol) of Compound **1**, along with 91 mg of Pd(PPh₃)₂Cl₂ and 39 mg of CuI, were added to a 100 mL round-bottom flask, evacuated, and filled with nitrogen gas, and this process was repeated three times. Under nitrogen protection, 5 mL of freshly distilled THF and 1.1 mL (7.96 mmol) of Et₃N were added, followed by slow dropwise addition of 2.63 g (5.16 mmol) of Compound **2** dissolved in 5 mL of THF, with a controlled drip time within one hour. After stirring the reaction at room temperature for 24 h, the reaction mixture was filtered through a short column of silica gel to remove the precipitate. The filtrate was rotary evaporated to remove the solvent and purified by petroleum ether through a silica gel column. This yielded 3.85 g of product (colorless transparent liquid) with a yield of 98%. ¹H NMR δ (ppm): 8.48 (s, 2H), 7.69 (s, 2H), 7.54 (d, 1H), 7.52 (d, 1H), 7.40 (dd, 1H), 7.34 (dd, 1H), 4.27 (t, 2H), 4.01 (t, J = 6 Hz, 2H), 1.87 (p, J = 6 Hz, 4H), 1.65–1.25 (m, 20H), 0.91 (t, J = 6 Hz, 6H), and 0.24 (s, 9H).

Synthesis of PECz: 8.30 g (10.9 mmol) of Compound **3** was added to a 250 mL two-neck flask, evacuated, and filled with nitrogen gas, repeating this process three times. Separately, a mixture of 8 mL tetrahydrofuran and 44 mL methanol solvent was bubbled with nitrogen gas to remove oxygen for 30 min and then added to the aforementioned two-neck flask. After thorough mixing and dissolution, 3.3 mL of 20% KOH aqueous solution was added. The reaction proceeded at room temperature under nitrogen protection for 2 h. Upon completion of the reaction, the mixture was filtered through a short column of silica gel, followed by rotary evaporation to remove the solvent. The crude product was purified using petroleum ether through a silica gel column. This yielded 7.36 g of white crystals with a yield of 98%. ¹H NMR δ (ppm): 8.48 (s, 2H), 7.69 (s, 2H), 7.54 (d, 1H), 7.52 (d, 1H), 7.40 (dd, 1H), 7.34 (dd, 1H), 4.27 (t, 2H), 4.05 (t, J = 6 Hz, 2H), 3.28 (s, 1H), 1.87 (p, J = 6 Hz, 4H), 1.65–1.25 (m, 20H), and 0.91 (t, J = 6 Hz, 6H).

Synthesis of *hb*-PPECz: 19.8 mg of 1,2-diiodobenzene (0.06 mmol), 63 mg of Pd(PPh₃)₂Cl₂, 48 mg of triphenylphosphine, and 42 mg of CuI were added to a 25 mL two-neck flask equipped with a dropping funnel, and the process of vacuum evacuation and nitrogen gas purging was repeated three times. A mixture of 7.5 mL of toluene and 7.5 mL of triethylamine, degassed by three freeze–pump–thaw cycles, was added. The resulting reaction mixture was heated to 90 °C. Then, a solution of 2.07 g (3 mmol) PECz in 7.5 mL toluene, degassed by three freeze–pump–thaw cycles, was added dropwise to the reaction mixture at a rate of 1 drop per 40 s. After stirring for 48 h, the reaction mixture was filtered through a short silica gel column. The filtrate was then rotary evaporated to remove the solvent. Subsequently, 10 mL of chloroform was added to dissolve the solid, and then methanol was used to precipitate and separate the polymer *hb*-PPECz. The polymer was purified by two rounds of dissolution and precipitation, yielding a tan solid weighing 1.01 g.

Synthesis of *c*-PPECz-1: 100 mg of *hb*-PPECz, 8 mg of palladium acetate, and 13.4 mg of (O-tolyl)₃P were added to a 25 mL single-neck flask, and the process of vacuum evacuation and nitrogen purging was repeated three times. Then, a solution of 5 mL toluene, 0.4 mL triethylamine, and 0.0163 g divinylbenzene, degassed by three freeze–pump–thaw cycles, was added. The reaction mixture was then heated to 90 °C and allowed to react for 48 h. After cooling to room temperature under stirring, the reaction mixture was added dropwise to methanol to precipitate the product. The product was dried under vacuum to give *c*-PPECz-1, 0.095 g.

Synthesis of *c*-PPECz-2~*c*-PPECz-5: *c*-PPECz-2~*c*-PPECz-4 were synthesized under the same conditions of *c*-PPECz-1 except for the concentration of *hb*-PPECz. *c*-PPECz-5 was synthesized under the same conditions as *c*-PPECz-3 except for the addition of 10 mg PVP K-30.

3. Results and Discussion

3.1. Synthesis of Hyperbranched Conjugated Prepolymer *hb*-PPECz

As shown in Scheme 1, an AB₂-type monomer (3-((3,5-dibromo-4-(octyloxy)phenyl)ethynyl)-6-ethynyl-9-octyl-9H-carbazole, PECz) containing one ethynyl group and two -Br groups was synthesized. Due to the significant reactivity difference between -Br and -I groups, the Sonogashira reaction of Compound 1 with Compound 2 selectively occurred between ethynyl and -I groups, leaving the -Br groups unreacted. With sequential deprotection, the AB₂-type monomer PECz was obtained. The ¹H NMR spectrum of PECz and peak assignments are shown in Figure 1A. Peaks corresponding to the protons of -C≡CH(a), -N-CH₂-(b), -OCH₂-(c), phenyl(d, e, f, g), and -(CH₂)₆CH₃(h, h') can be observed. The integral ratio of a/b/c/d/e/f/g = 1/2/2/2/2/2/2, which is consistent with the theoretical value, indicating the successful synthesis of monomer PECz.

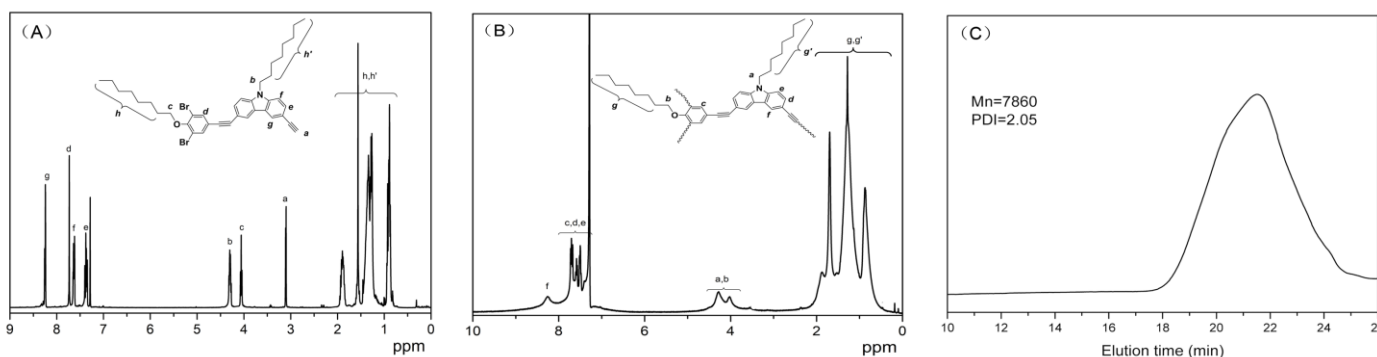


Figure 1. (A) ¹H NMR spectrum of AB₂ monomer PECz; (B) ¹H NMR spectrum of hyperbranched prepolymer *hb*-PPECz; (C) GPC curve of hyperbranched prepolymer *hb*-PPECz.

The monomer PECz was polymerized by the Sonogashira reaction to give the hyperbranched conjugated prepolymer *hb*-PPECz. For the polymerization of AB_n monomer to give hyperbranched polymer, core molecules were usually added to control the product's molecular weight by varying the molar ratio of [AB_n monomer]/[core molecule] and obtain a narrower molecular weight distribution [25]. Therefore, 1,4-diiodobenzene was added as the core molecule. The ¹H NMR spectrum of *hb*-PPECz and its peak assignments are shown in Figure 1B. No signal of -C≡CH can be observed, indicating the complete conversion of -C≡CH. As reported in a previous paper on the synthesis of hyperbranched poly(*m*-phenyleneethynylene-*alt*-*p*-phenyleneethynylene) (*hb*-PMPE) [25], the signal of -OCH₂- in dendritic (D), terminal (T), and linear (L) units of *hb*-PMPE can be distinguished as three separated peaks within the range of δ 4.0~4.4 ppm in the ¹H NMR spectrum, since the chemical environment of the alkoxy group in D, T, and L units of *hb*-PMPE is different from each other: in the D unit, both the two o-substituent groups of alkoxy are ethynylene groups; in the T unit, both the two o-substituent groups of alkoxy are bromide groups; while in the L unit, one o-substituent group is ethynylene and another is bromide. Therefore, the branching degree (DB) of *hb*-PMPE can be calculated from the ¹H NMR spectrum by the integration of these three peaks. But for *hb*-PPECz, we cannot calculate the DB from the ¹H NMR spectrum since the signals of -OCH₂- in D, T, and L units are partially overlapped by the signal of -NCH₂-.

3.2. Photophysical and Electrochemical Properties of Hyperbranched Prepolymer *hb*-PPECz

The photophysical and electrochemical properties significantly affect the performance of CMPs for applications in the fields of clean energy [27]. To evaluate the potential application in the field of clean energy, the photophysical and electrochemical properties of *hb*-PPECz were investigated by UV-vis absorbance, luminescence, and cyclic voltammetry

(CV), respectively. The normalized UV-vis absorbance and luminescence ($\lambda_{\text{ex}} = 313 \text{ nm}$) spectra of *hb*-PPECz are shown in Figure 2A,B, respectively. The UV-vis absorption spectrum shows a major band (λ_{max} at 313 nm) with a significant shoulder peak (λ_{sh} at 345 nm). The luminescence spectrum of *hb*-PPECz shows a major band with λ_{max} at 483 nm, emitting blue light under 365 nm irradiation. The optical energy bandgap (E_g^{opt}) can be estimated from the onset absorption wavelength (λ_{onset}) by the formula $E_g^{\text{opt}} = 1240/\lambda_{\text{onset}}$. The E_g^{opt} of *hb*-PPECz was 2.98 eV.

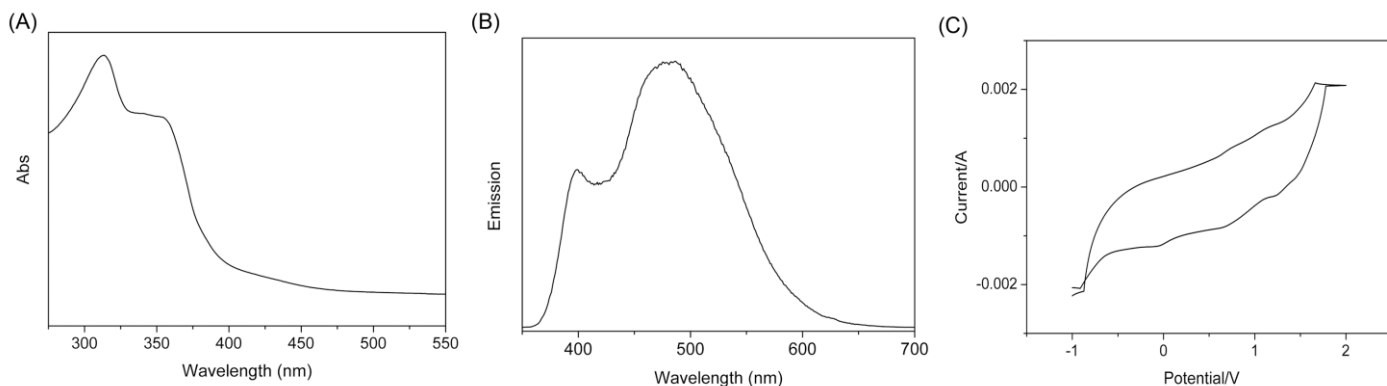


Figure 2. (A) Normalized UV-vis absorption spectrum of *hb*-PPECz in THF solution. (B) Normalized luminescent spectrum of *hb*-PPECz in THF solution ($\lambda_{\text{ex}} = 313 \text{ nm}$). (C) Cyclic voltammetry curve of *hb*-PPECz in CH_2Cl_2 solution.

To gain further insight into the electronic properties, cyclic voltammetry (CV) measurements were conducted to reveal the energy band structure of *hb*-PPECz. The CV curve of *hb*-PPECz is shown in Figure 2C. HOMO and LUMO energy levels of *hb*-PPECz were -5.81 eV and -2.83 eV , which were calculated from its oxidation potential ($E_{\text{pa(onset)}} = 1.05 \text{ eV}$) by the following formulas:

$$E_{\text{HOMO}} = -4.84 \text{ eV} - E_{\text{pa(onset)}}, \quad (1)$$

$$E_{\text{LUMO}} = E_g^{\text{opt}} - |E_{\text{HOMO}}| \quad (2)$$

in which E_{HOMO} stands for the HOMO energy level, E_{LUMO} stands for the LUMO energy level, and $E_{\text{pa(onset)}}$ stands for the onset oxidation potential. The standard hydrogen electrode (NHE) potential is referenced to the vacuum energy level as -4.5 eV , and in this experiment, a mercury–silver amalgam electrode (in a 0.1 M KCl solution) is used as the reference electrode, with a potential relative to NHE of 0.34 eV .

A low energy gap is a desired characteristic for high-performance CMPs. A lower energy gap means longer conjugation length and higher conductivity. Due to the long conjugation length composed of phenyl, ethynyl, and carbazole units for *hb*-PPECz, the energy gap of *hb*-PPECz is relatively low and makes *hb*-PPECz potential applications in clean energy areas such as electrode materials and electrocatalysts.

3.3. Synthesis and Pore Structure Characterization of Multiple Micro-/Meso-Porous Conjugated Polymer *c*-PPECz

The hyperbranched prepolymer *hb*-PPECz carries an aromatic -Br group in each of its branch ends. Therefore, post-crosslinking of *hb*-PPECz was carried out by Heck reaction with divinyl benzene (DVB) to give a crosslinked conjugated polymer (*c*-PPECz). Due to the free volume between the branches of *hb*-PPECz and crosslinked conjugated skeleton, *c*-PPECz should contain micro-/meso-pores. The effects of the concentration of *hb*-PPECz and added dispersant (PVP K-30) on the morphology and porosity of *c*-PPECz were investigated. The post-crosslinking conditions and product appearance are shown in Table 1. With a higher concentration of *hb*-PPECz (4 wt/v%), the bulky gel was obtained. Within the range of 0.6 wt/v%~2 wt/v%, turbid dispersions were obtained.

Table 1. Post-crosslinking conditions for Heck reaction of *hb*-PPECz with DVB.

	<i>c</i> -PPECz-1	<i>c</i> -PPECz-2	<i>c</i> -PPECz-3	<i>c</i> -PPECz-4	<i>c</i> -PPECz-5 *
[<i>hb</i> -PPECz] (wt/v%)	2	0.6	1	4	1
product appearance	dispersion	dispersion	dispersion	bulky gel	dispersion

Other conditions: *hb*-PPECz, 0.1 g; DVB, 0.0134 g; palladium acetate, 8 mg; $(O\text{-tolyl})_3\text{P}$, 13.4 mg; in Tol; 90 °C; 48 h.

* Added PVP K-30: 10 wt% of *hb*-PPECz.

The SEM images of *c*-PPECzs are shown in Figure 3. Except for *c*-PPECz-4 (Figure 3D), the other four *c*-PPECzs were mainly composed of nano-sized particles, with a particle size of approximately 200~300 nm; however, significant bonding between the particles can be observed in Figure 3A–C. By comparing Figure 3A–C, there is no significant change in the particle size with increasing concentration of *hb*-PPECz. However, a significant effect of concentration on the shape regularity of the particles can be observed. Under the concentration of 1 wt/v%, spherical-like particles (*c*-PPECz-3) were obtained. In radical dispersion polymerizations [24,28], a dispersant was added to prevent aggregation and control the morphology of polymerization products. Therefore, the effect of dispersant PVP K-30 on the morphology of *c*-PPECz was investigated under the concentration of 1 wt/v%. The result showed that by the addition of PVP (10 wt% of *hb*-PPECz), the shape of product particles became more regular, and most of the particles were nearly spherical (Figure 3E).

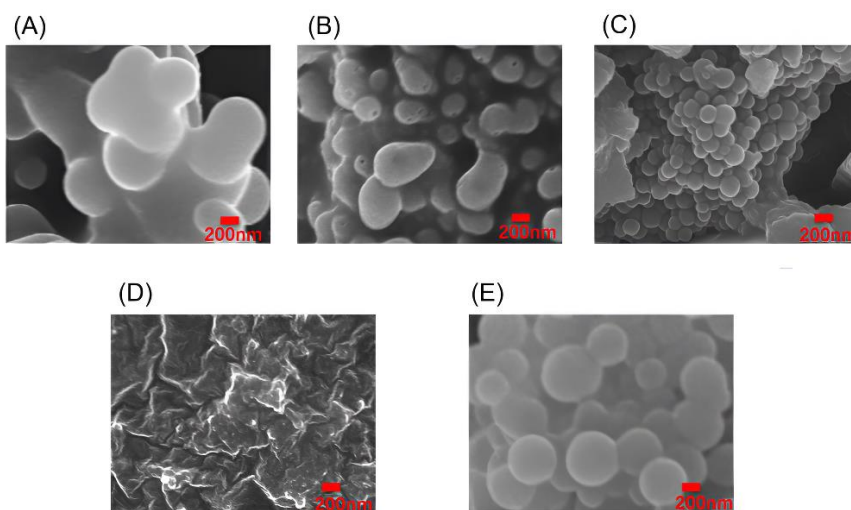


Figure 3. SEM images of crosslinked conjugated polymer *c*-PPECzs: (A) *c*-PPECz-1; (B) *c*-PPECz-2; (C) *c*-PPECz-3; (D) *c*-PPECz-4; (E) *c*-PPECz-5.

The pore structure and microporous characteristics of *c*-PPECzs were investigated by the N_2 adsorption–desorption isotherms at a temperature of 77.4 K, as shown in Figure 4. The vertical axis of the adsorption–desorption isotherm is represented by $\Sigma V(\text{STP})$ (cm^3/g), indicating the adsorption amount under standard conditions. It can be observed that the adsorption curve of each *c*-PPECz shows a large slope at low pressure ($P/P_0 < 0.1$), exhibiting typical characteristics of microporous materials. Based on the adsorption–desorption isotherm data, pore structure information of the sample is obtained through computational analysis, and the pore size distribution is determined using the BJH (Barret–Joyner–Halenda) method. The BET equation is employed to determine the specific surface area of the sample, while the total pore volume and average pore diameter are calculated from the nitrogen adsorption amount at a relative pressure of 0.990. The BET specific surface area, total pore volume, average pore diameter, and the percentage of pore size below 10 nm for the *c*-PPECzs are presented in Table 2. Additionally, based on the N_2 adsorption–desorption isotherms, pore size distribution curves are obtained using the Barret–Joyner–Halenda method, as illustrated in Figure 5. The vertical axis, represented by dV/dD ($\text{mL}/\text{nm}/\text{g}$), signifies the increment of the pore volume.

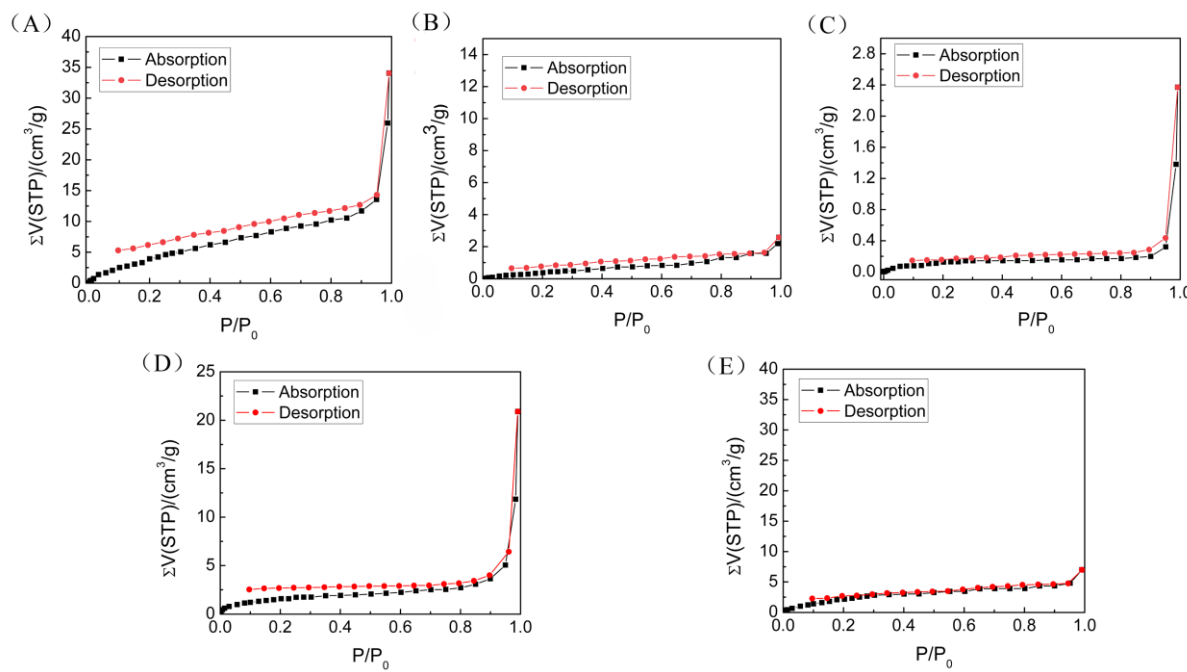


Figure 4. N_2 adsorption and desorption curves of *c*-PPECzs: (A) *c*-PPECz-1; (B) *c*-PPECz-2; (C) *c*-PPECZ-3; (D) *c*-PPECz-4; (E) *c*-PPECz-5.

Table 2. Pore characteristics of *c*-PPECzs.

	BET Specific Surface Area/ $(m^2 \cdot g^{-1})$	Pore Volume/ $(cm^3 \cdot g^{-1})$	Average Pore Size/nm	Percentage of Pore Size below 10 nm
<i>c</i> -PPECz-1	15.7014	0.0476	12.1263	83.24%
<i>c</i> -PPECz-2	1.4085	0.0034	9.6557	93.72%
<i>c</i> -PPECz-3	0.3207	0.0032	39.9100	54.39%
<i>c</i> -PPECz-4	5.9429	0.0306	20.5960	58.73%
<i>c</i> -PPECz-5	10.7781	0.0108	4.0081	94.47%

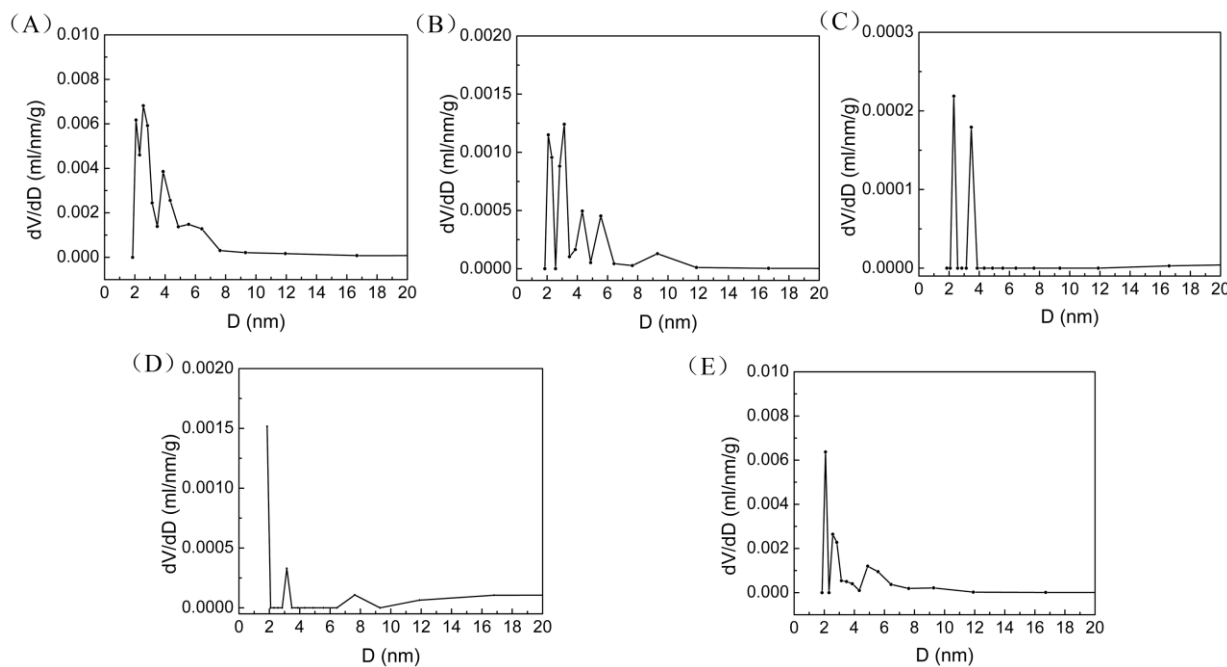


Figure 5. Pore size distribution curves of *c*-PPECzs: (A) *c*-PPECZ-1; (B) *c*-PPECz-2; (C) *c*-PPECz-3; (D) *c*-PPECz-4; (E) *c*-PPECz-5.

Comparing *c*-PPECz-1 with *c*-PPECz-4 shows that under a higher *hb*-PPECz concentration of 4 wt/v%, the reaction exhibits a gel phenomenon, the pore area percentage is smaller, and the specific surface area is reduced. Comparing *c*-PPECZ-3 with *c*-PPECZ-5 shows that the addition of dispersant PVP K30 results in smaller pore size, higher pore content, and a significant increase in specific surface area. The results showed that the addition of PVP K-30 was not only conducive to obtaining spherical particles but also conducive to increasing the micropore/mesopore content and specific surface area. Moreover, the results show that *c*-PPECzs have multiple porous structures mainly constructed by micropores and mesopores. This multiple porous structure is particularly beneficial for electrode materials. Micropores promote charge enrichment, while mesopores promote charge transfer, electrolyte penetration, and mass transfer [29].

3.4. Loading of Metal Ion in *c*-PPECz

For certain applications, doping of metal ions in CMPs can significantly improve the performance of CMPs [30–32]. The obtained *c*-PPECz contains abundant coordination sites, including C≡C bonds and heteroatoms of O and N. These coordination sites can easily bind with metallic ions and make them homogeneously dispersed in CMPs, hence improving the performance of CMPs as electrode materials and electrocatalysts by increasing the conductivity and content of active metal species of CMPs [33]. Therefore, as examples, the loading of Zn²⁺ and Ni²⁺ ions in *c*-PPECz was investigated. ZnCl₂ and NiSO₄ were dissolved in distilled water to prepare a metal ion solution with a concentration of 400 mg·L⁻¹. A total of 10 mg of *c*-PPECz-5 was suspended in 20 mL of the metal ion solution. The mixture was then sealed and allowed to stand at room temperature for 24 h. After adsorption, the adsorbent was separated from the solution by filtration, and the filtrate was collected for analysis using a UV-visible spectrophotometer. The results are shown in Figure 6. The adsorption capacity q_e (mg·g⁻¹) was calculated according to the following formula:

$$q_e = \frac{V \times (c_0 - c_e)}{W} \quad (3)$$

in which V represents the volume of the metal ion solution (L), c_0 represents the initial concentration of the metal ion solution (mg·L⁻¹), c_e represents the concentration of the metal ions after adsorption (mg·L⁻¹), and W represents the mass of *c*-PPECz (g). The adsorption capacity of *c*-PPECz-5 for Zn(II) was 206 mg·g⁻¹, and for Ni(II), it was 523 mg·g⁻¹.

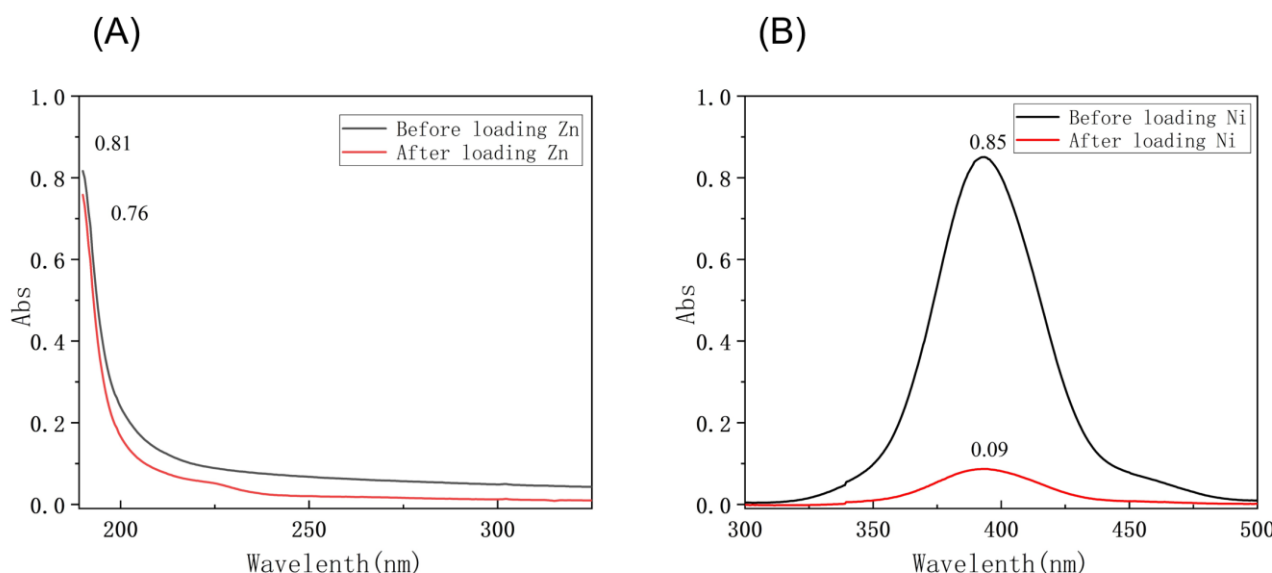


Figure 6. UV spectra of metal ion solutions: (A) Zn(II); (B) Ni(II).

4. Conclusions

A nano-structured conjugated polymer (*c*-PPECz) with multiple micro-/meso-pores was synthesized by the post-crosslinking Heck reaction of DVB with *hb*-PPECz, which was synthesized by an AB₂ monomer (3-((3,5-dibromo-4-(octyloxy)phenyl)ethynyl)-6-ethynyl-9-octyl-9H-carbazole, PECz). The *hb*-PPECz concentration and added dispersant PVP K30 in the post-crosslinking reaction showed significant effects on the morphology and porosity of *c*-PPECz. Lower *hb*-PPECz concentration was beneficial for obtaining nano-structured products. The addition of dispersant PVP K-30 was not only conducive to obtaining spherical particles but also conducive to increasing the micropore/mesopore content and specific surface area. Nearly spheric nanoparticles (200~300 nm) (*c*-PPECz-5) with multiple porous structures mainly constructed by micropores and mesopores were obtained under the concentration of 1 wt/v% in the presence of PVP K-30 (10 wt% of *hb*-PPECz). The combination of multiple micro-/meso-porous structures, relatively low energy gap, and abundant coordination sites provides the obtained *c*-PPECzs with potential applications in the fields of clean energy, such as electrode materials and electrocatalysts.

Author Contributions: All authors contributed meaningfully to this study. Conceptualization, H.L.; methodology, Z.L.; software, Z.L.; validation, Z.L.; investigation, Z.L.; writing—original draft preparation, H.L. and Z.L.; writing—review and editing, H.L. and Z.L.; supervision, H.L.; funding acquisition, H.L. All authors have read and agreed to the published version of the manuscript.

Funding: This research received no external funding.

Institutional Review Board Statement: Not applicable.

Data Availability Statement: Data are contained within the article.

Acknowledgments: The authors express gratitude to the editors and the reviewers for their constructive and helpful review comments.

Conflicts of Interest: The authors declare no conflicts of interest.

References

1. Amin, K.; Ashraf, N.; Mao, L.; Faul, C.F.; Wei, Z. Conjugated microporous polymers for energy storage: Recent progress and challenges. *Nano Energy* **2021**, *85*, 105958. [[CrossRef](#)]
2. Luo, S.; Zeng, Z.; Wang, H.; Xiong, W.; Song, B.; Zhou, C.; Duan, A.; Tan, X.; He, Q.; Zeng, G.; et al. Recent progress in conjugated microporous polymers for clean energy: Synthesis, modification, computer simulations, and applications. *Prog. Polym. Sci.* **2021**, *115*, 101374. [[CrossRef](#)]
3. Luo, S.; Zeng, Z.; Zeng, G.; Liu, Z.; Xiao, R.; Xu, P.; Wang, H.; Huang, D.; Liu, Y.; Shao, B.; et al. Recent advances in conjugated microporous polymers for photocatalysis: Designs, applications, and prospects. *J. Mater. Chem. A* **2020**, *8*, 6434–6470. [[CrossRef](#)]
4. Yang, L.; Ma, Y.; Xu, Y.; Chang, G. Cation- π -induced lithium-doped conjugated microporous polymer with remarkable hydrogen storage performance. *Chem. Commun.* **2019**, *55*, 11227–11230. [[CrossRef](#)] [[PubMed](#)]
5. Yuan, S.; Dorney, B.; White, D.; Kirklin, S.; Zapol, P.; Yu, L.; Liu, D.-J. Microporous polyphenylenes with tunable pore size for hydrogen storage. *Chem. Commun.* **2010**, *46*, 4547–4549. [[CrossRef](#)]
6. Zeng, W.; Zhang, Y.; Zhao, X.; Qin, M.; Li, X.; Jin, W.; Zhang, D. One-pot synthesis of conjugated microporous polymers based on extended molecular graphenes for hydrogen storage. *Polymer* **2019**, *174*, 96–100. [[CrossRef](#)]
7. Sun, C.-J.; Wang, P.-F.; Wang, H.; Han, B.-H. All-thiophene-based conjugated porous organic polymers. *Polym. Chem.* **2016**, *7*, 5031–5038. [[CrossRef](#)]
8. Qiao, S.; Wei, H.; Wang, T.; Huang, W.; Gu, C.; Yang, R.; Li, X. A ribbon-like ultramicroporous conjugated polycarbazole network for gas storage and separation. *New J. Chem.* **2016**, *40*, 3172–3176. [[CrossRef](#)]
9. Qiao, S.; Huang, W.; Du, Z.; Chen, X.; Shieh, F.-K.; Yang, R. Phosphine oxide-based conjugated microporous polymers with excellent CO₂ capture properties. *New J. Chem.* **2015**, *39*, 136–141. [[CrossRef](#)]
10. Broicher, C.; Foit, S.R.; Rose, M.; Hausoul, P.J.; Palkovits, R. A bipyridine-based conjugated microporous polymer for the Ir-catalyzed dehydrogenation of formic acid. *ACS Catal.* **2017**, *7*, 8413–8419. [[CrossRef](#)]
11. Okubo, M.; Hosono, E.; Kim, J.; Enomoto, M.; Kojima, N.; Kudo, T.; Zhou, H.; Honma, I. Nanosize effect on high-rate Li-ion intercalation in LiCoO₂ electrode. *J. Am. Chem. Soc.* **2007**, *129*, 7444–7452. [[CrossRef](#)]
12. Zhang, Q.; Dai, Q.; Li, M.; Wang, X.; Li, A. Incorporation of MnO nanoparticles inside porous carbon nanotubes originated from conjugated microporous polymers for lithium storage. *J. Mater. Chem. A* **2016**, *4*, 19132–19139. [[CrossRef](#)]
13. Chen, Y.; Li, H.; Tang, M.; Zhuo, S.; Wu, Y.; Wang, E.; Wang, S.; Wang, C.; Hu, W. Capacitive conjugated ladder polymers for fast-charge and-discharge sodium-ion batteries and hybrid supercapacitors. *J. Mater. Chem. A* **2019**, *7*, 20891–20898. [[CrossRef](#)]

14. Liao, Y.; Wang, H.; Zhu, M.; Thomas, A. Efficient supercapacitor energy storage using conjugated microporous polymer networks synthesized from Buchwald–Hartwig coupling. *Adv. Mater.* **2018**, *30*, 1705710. [[CrossRef](#)] [[PubMed](#)]
15. Roy, S.; Bandyopadhyay, A.; Das, M.; Ray, P.P.; Pati, S.K.; Maji, T.K. Redox-active and semi-conducting donor–acceptor conjugated microporous polymers as metal-free ORR catalysts. *J. Mater. Chem. A* **2018**, *6*, 5587–5591. [[CrossRef](#)]
16. Liu, W.; Wang, K.; Wang, C.; Liu, W.; Pan, H.; Xiang, Y.; Qi, D.; Jiang, J. Mixed phthalocyanine-porphyrin-based conjugated microporous polymers towards unveiling the activity origin of Fe–N₄ catalysts for the oxygen reduction reaction. *J. Mater. Chem. A* **2018**, *6*, 22851–22857. [[CrossRef](#)]
17. Rao, K.V.; Halder, R.; Maji, T.K.; George, S.J. Dynamic, conjugated microporous polymers: Visible light harvesting via guest-responsive reversible swelling. *Phys. Chem. Chem. Phys.* **2016**, *18*, 156–163. [[PubMed](#)]
18. Yu, Y.-Y.; Tsai, T.-W.; Chen, C.-P. Efficient ternary organic photovoltaics using two conjugated polymers and a nonfullerene acceptor with complementary absorption and cascade energy-level alignment. *J. Phys. Chem. C* **2018**, *122*, 24585–24591. [[CrossRef](#)]
19. Xu, Y.; Chen, L.; Guo, Z.; Nagai, A.; Jiang, D. Light-emitting conjugated polymers with microporous network architecture: Interweaving scaffold promotes electronic conjugation, facilitates exciton migration, and improves luminescence. *J. Am. Chem. Soc.* **2011**, *133*, 17622–17625. [[CrossRef](#)]
20. Jiang, J.-X.; Trewin, A.; Adams, D.J.; Cooper, A.I. Band gap engineering in fluorescent conjugated microporous polymers. *Chem. Sci.* **2011**, *2*, 1777–1781. [[CrossRef](#)]
21. Gu, C.; Huang, N.; Chen, Y.; Qin, L.; Xu, H.; Zhang, S.; Li, F.; Ma, Y.; Jiang, D. π -conjugated microporous polymer films: Designed synthesis, conducting properties, and photoenergy conversions. *Angew. Chem.* **2015**, *127*, 13798–13802. [[CrossRef](#)]
22. Gu, C.; Huang, N.; Chen, Y.; Zhang, H.; Zhang, S.; Li, F.; Ma, Y.; Jiang, D. Porous organic polymer films with tunable work functions and selective hole and electron flows for energy conversions. *Angew. Chem. Int. Ed.* **2016**, *55*, 3049–3053. [[CrossRef](#)]
23. Downey, J.S.; Frank, R.S.; Li, W.-H.; Stöver, H.D. Growth mechanism of poly (divinylbenzene) microspheres in precipitation polymerization. *Macromolecules* **1999**, *32*, 2838–2844. [[CrossRef](#)]
24. Almog, Y.; Reich, S.; Levy, M. Monodisperse polymeric spheres in the micron size range by a single step process. *Br. Polym. J.* **1982**, *14*, 131–136. [[CrossRef](#)]
25. Wang, B.; Tan, Q.; Lu, J.; Liang, H. Facile synthesis of hyperbranched poly (p-phenyleneethynylene-alt-m-phenyleneethynylene) with narrow dispersity and high branching degree by sonogashira polymerization of an AB₂ monomer. *J. Polym. Sci. Part A Polym. Chem.* **2018**, *56*, 96–104. [[CrossRef](#)]
26. Vives, G.; Guerrero, J.M.; Godoy, J.; Khatua, S.; Wang, Y.-P.; Kiappes, J.; Link, S.; Tour, J.M. Synthesis of fluorescent dye-tagged nanomachines for single-molecule fluorescence spectroscopy. *J. Org. Chem.* **2010**, *75*, 6631–6643. [[CrossRef](#)]
27. Hayat, A.; Sohail, M.; El Jery, A.; Al-Zaydi, K.M.; Raza, S.; Ali, H.; Al-Hadeethi, Y.; Taha, T.A.; Din, I.U.; Khan, M.A.; et al. Recent advances in ground-breaking conjugated microporous polymers-based materials, their synthesis, modification and potential applications. *Materials Today* **2023**, *64*, 180–208. [[CrossRef](#)]
28. Barrett, K.E. Dispersion polymerisation in organic media. *Br. Polym. J.* **1973**, *5*, 259–271. [[CrossRef](#)]
29. Parlett, C.M.; Wilson, K.; Lee, A.F. Hierarchical porous materials: Catalytic applications. *Chem. Soc. Rev.* **2013**, *42*, 3876–3893. [[CrossRef](#)]
30. Zhang, Q.; Ge, S.; Wang, X.; Sun, H.; Zhu, Z.; Liang, W.; Li, A. Novel MnO/conjugated microporous polymer derived-porous hard carbon nanocomposite for superior lithium storage. *RSC Adv.* **2014**, *4*, 41649–41653. [[CrossRef](#)]
31. Mu, P.; Sun, H.; Zhu, Z.; Liang, W.; Liu, J.; Li, A. Synthesis and Properties of Nitrogen-Containing Conjugated Microporous Polymers. *Macromol. Mater. Eng.* **2016**, *301*, 451–456. [[CrossRef](#)]
32. Zhang, Q.; Meng, Y.; Li, M.; Wang, X. Thiophene containing conjugated microporous polymers derived sulfur-enriched porous carbon supported Fe₃O₄ nanoparticles with superior lithium storage properties. *J. Mater. Sci. Mater. Electron.* **2019**, *30*, 1425–1433. [[CrossRef](#)]
33. Zhang, B.; Wang, W.; Liang, L.; Xu, Z.; Li, X.; Qiao, S. Prevailing conjugated porous polymers for electrochemical energy storage and conversion: Lithium-ion batteries, supercapacitors and water-splitting. *Coord. Chem. Rev.* **2021**, *436*, 213782. [[CrossRef](#)]

Disclaimer/Publisher’s Note: The statements, opinions and data contained in all publications are solely those of the individual author(s) and contributor(s) and not of MDPI and/or the editor(s). MDPI and/or the editor(s) disclaim responsibility for any injury to people or property resulting from any ideas, methods, instructions or products referred to in the content.